Spectrochimica Acta Part A: Molecular and Biomolecular Spectroscopy 121 (2014) 605–612

Contents lists available at ScienceDirect

Spectrochimica Acta Part A: Molecular and Biomolecular Spectroscopy

journal homepage: www.elsevier.com/locate/saa

Study on polymer fibers doped with phosphorescent Re(I) complex via electrospinning: Synthetic strategy, structure, morphology and photophysical features

Wang Dejin [a,*], Liu Qiang [b], Wang Fei [b]

[a] *School of Resources and Environment, Anqing Normal University, Anqing 246052, PR China*
[b] *Shanghai University, Shanghai 200444, PR China*

HIGHLIGHTS

- A Re(I) complex owing oxadiazole derived ligand was synthesized.
- Its single crystal structure and electronic nature were investigated.
- It was doped into a polymer matrix to construct composite fibers.
- The photophysical features of pure sample and doped sample were compared.
- The doped sample showed better performance by restraining geometric relaxation.

GRAPHICAL ABSTRACT

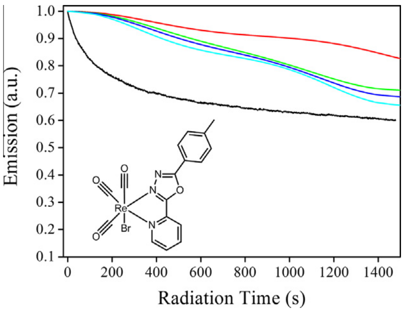

ARTICLE INFO

Article history:
Received 13 October 2013
Received in revised form 2 November 2013
Accepted 5 November 2013
Available online 13 November 2013

Keywords:
Re complex
Photoluminescence
Microfiber
Crystal

ABSTRACT

In the following paper, a Re(I) complex with electron-withdrawing oxadiazole group in its diamine ligand (denoted as N–N) was synthesized. Its single crystal structure analysis confirmed the successful synthesis of both ligand and complex. The central Re(I) ion localized in a traditional octahedral coordination environment. The diamine ligand 2-(pyridin-2-yl)-5-(p-tolyl)-1,3,4-oxadiazole (denoted as PPOZ) took a coplanar structure and the corresponding face-to-face π–π attraction between PPOZ ligands made the Re(I) complex molecules adjust a highly ordered arrangement which was positive to improve emissive performance. In order to repress the excited state geometric relaxation and further improve the emissive performance, the Re(I) complex was doped into a polymer host poly(vinylpyrrolidone) via electrospinning, resulting in composite fibers. The morphology of those composite fibers was analyzed by electron microscopy. The photophysical comparison between bulk sample and composite fibers indicated that the composite fibers showed emission blue shift, longer excited state lifetime and improved photostability. Further analysis suggested that the excited state geometric relaxation could be effectively repressed when the Re(I) complex molecules were immobilized in the polymer matrix, leading to above variations.

Introduction

One-dimensional nanostructures such as nanowires and nanofibers have been demonstrated to be promising candidates owing to their potential optoelectronic and mechanical features [1]. Among the developed techniques for constructing those nanostructures, electrospinning has been proved to be a charming one because of its low cost, simple and easy-to-go constructing route. The obtained electrospinning fibers usually own large surface-to-volume ratio, controllable morphology and feasible mechanical strength, making themselves a potential supporting host for various optoelectronic systems [2–6].

---

[*] Corresponding author. Tel.: +86 0556 5501280.
E-mail address: wang_dj01@163.com (W. Dejin).

http://dx.doi.org/10.1016/j.saa.2013.11.022

To achieve satisfactory photophysical performance, some opto-electronic dopants such as organic dyes and transition metal complexes have been doped into the electropinning fibers, which widens the application of these composite fibers [7,8]. As a class of typical phosphorescent material, Re(I) complexes with general molecular formula of $Re(CO)_3(N–N)X$ have been widely studied since they own good photoluminescence (PL) yield, controllable emissive wavelength and enough stability [9–11], where N–N and X mean diamine ligand and halogen atom, respectively. Theoretical calculation on them suggests that the photoinduced excitations and emissions involve electronic transitions between frontier molecular orbitals (FMOs). The occupied FMOs are usually composed of metal ion and halogen atom, while the unoccupied FMOs are π^* orbitals in nature. The excited state and the corresponding emissive state are thus assigned as a mixed character of metal-to-ligand-charge-transfer and ligand-to-ligand-charge-transfer (ML&LLCT) [11–15].

The systematical analysis by Zhang and coworkers on the MLCT excited state of a series of transition metal complexes suggests that the MLCT excited state, as well as the emissive performance of corresponding metal complexes, is related with the geometric relaxation of MLCT excited state [12–15]. Both emissive energy and emission quantum yield can be improved upon effective repression of geometric relaxation. Some approved solutions include using N–N ligands with large steric hindrance and the immobilization into solid matrixes such as polymer matrix or silica molecular sieves [12–15]. In addition, it has been found that the existence of electron-withdrawing group in N–N ligand is positive to improve emissive performance of corresponding Re(I) complexes [15]. It is thus expected that the emissive performance of Re(I) complex with electron-withdrawing group in its N–N ligand can be further improved when it is immobilized in solid matrix.

Encouraged by above results and considerations, in this paper, we design and synthesize a N–N ligand 2-(pyridin-2-yl)-5-(p-tolyl)-1,3,4-oxadiazole (denoted as PPOZ) which owns an electron-withdrawing group in its molecular structure and its corresponding Re(I) complex $Re(CO)_3(PPOZ)Br$. The composite electrospinning fibers are also constructed using a polymer as the host and $Re(CO)_3(PPOZ)Br$ as the photo-active dopant. $Re(CO)_3(PPOZ)Br$ and the composite fibers are carefully characterized and studied. Their photophysical comparison is also performed to analyze the geometric relaxation of MLCT excited state and its correlation with emissive performance.

Experimental details

Scheme 1 demonstrates the synthetic and preparation procedure for the diamine ligand PPOZ, the Re(I) complex $Re(CO)_3(PPOZ)Br$ and the composite fibers (denoted as $PVP@Re(CO)_3(PPOZ)Br$). The initial reagent 2-(2H-tetrazol-5-yl)pyridine (denoted as TYP) was obtained through a literature procedure [16]. The other salts and organic chemicals, including 4-methylbenzoyl chloride, sodium azide, poly(vinylpyrrolidone) (PVP, K30), zinc bromide and $Re(CO)_5Br$, were bought from Alfresa Pharma Corporation and used as received without further purifications. The organic solvents used in this work, including CH_2Cl_2, $CHCl_3$, ethanol and N,N′-dimethyl formamide (DMF), were bought from Shanghai Chemical Cooperation and redistilled prior to use. The solvent water used in this work was deionized.

PPOZ diamine ligand

The diamine ligand PPOZ was synthesized following a literature procedure described as follows [16]. 10 mmol of TYP was slowly added into 20 mL of cold anhydrous pyridine under ice bath. Then 11 mmol of 4-methylbenzoyl chloride was also added into above solution slowly. The mixture was stirred for 20 min under ice bath and another 10 min at room temperature. Then the solution was heated to reflux under N_2 protection for two days. The solution was cooled to room temperature and then poured into 400 g of water ice. The resulting solid product was collected and further purified on a silica gel column (*n*-hexane: ethyl acetate (V:V) = 30:1). Yield: 50%. ^{1}HNMR ($CDCl_3$): δ 2.48 (3H, s), 7.37 (2H, d, J = 6.0), 7.49 (1H, t), 7.92 (1H, t), 8.14 (2H, d, J = 6.0), 8.33 (1H, d, J = 6.0), 8.86 (1H, d, J = 3.6). Anal. Calcd. For $C_{14}H_{11}N_3O$: C, 70.87; H, 4.67; N, 17.71. Found: C, 70.94; H, 4.83; N, 17.54.

$Re(CO)_3(PPOZ)Br$ complex

The Re(I) complex $Re(CO)_3(PPOZ)Br$ was synthesized following a literature procedure described as follows [17]. 0.5 mmol of PPOZ ligand and 0.5 mmol of $Re(CO)_5Br$ were added into 15 mL of anhydrous toluene. The solution was heated to reflux under N_2 protection overnight. Then the solvent was vaporized. The resulting solid product was collected and further purified on a silica gel column (*n*-hexane: ethyl acetate (V:V) = 30:1). Yield: 47%. ^{1}HNMR ($CDCl_3$): δ 2.51 (3H, s), 7.39 (2H, d, J = 6.0), 7.52 (1H, t), 7.95 (1H, t), 8.17 (2H, d, J = 6.0), 8.37 (1H, d, J = 6.0), 8.88 (1H, d, J = 3.6). Anal. Calcd. For $C_{17}H_{11}N_3O_4$: C, 34.76; H, 1.89; N, 7.15. Found: C, 34.57; H, 1.83; N, 7.34. Its identity is further confirmed by single crystal XRD analysis which will be discussed below.

$PVP@Re(CO)_3(PPOZ)Br$

$PVP@Re(CO)_3(PPOZ)Br$ composite fibers were prepared through electropinning technique as follows. Transparent solution of PVP dissolved in DMF was firstly prepared. Then finely measured $Re(CO)_3(PPOZ)Br$ was added into this solution to give

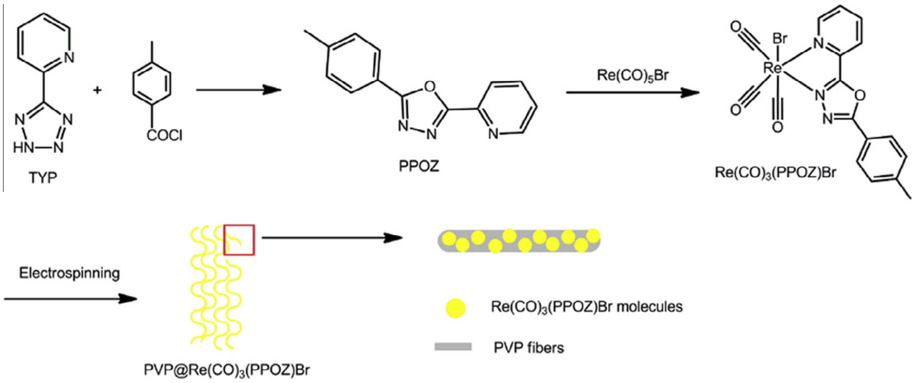

Scheme 1. The synthetic and preparation procedure for PPOZ, $Re(CO)_3(PPOZ)Br$ and $PVP@Re(CO)_3(PPOZ)Br$.

homogeneous solution which was then transferred into a 5 mL glass syringe equipped with a plastic needle (inner diameter = 0.6 mm) [18]. The end of a copper wire was connected to the anode terminal of a high-voltage generator, with the other end inserted into the polymer solution. A piece of Al foil was connected to the grounding electrode and placed beneath the plastic needle, serving as the collecting substrate. The tip-to-plate distance was 25 cm and the driving voltage was 18 kV.

Methods and measurements

^{1}H NMR spectra were measured by a Varian INOVA 300 spectrometer. The elemental analysis was finished on a Carlo Erba 1106 elemental analyzer. The single crystal analysis was finished by a Siemens P4 single-crystal X-ray diffractometer loaded with a Smart CCD-1000 detector at 298 K, using graphite-monochromated Mo Kα radiation. All hydrogen atoms were calculated. Absorption and emission spectra were measured in CH_2Cl_2 solutions (1 μM) by a HP 8453 UV–Vis–NIR diode array spectrophotometer and a Hitachi F-4500 fluorescence spectrophotometer, respectively. Emission decay dynamics were detected by a two-channel TEKTRONIX TDS-3052 oscilloscope, using pulsed Nd:yttrium aluminium garnet (YAG) laser (355 nm, the third-harmonic-generator pump) as the excitation source. Scanning electron microscopy (SEM) and fluorescence microscopy images were measured on a Hitachi S-4800 microscope and a Nikon TE2000-U fluorescence microscopy powered by a mercury lamp, respectively. Theoretical analysis on $Re(CO)_3$(PPOZ)Br, including the composition of the FMOs and the first ten singlet excitations, was performed by time dependent density functional theory (TD-DFT) using GAMESS at RB3PW91/SBKJC level in vacuum, with its crystal structure as the initial structure. The graphical presentation was generated by wxMacmolplt software package with contour value of 0.025. All measurements were carried out in the air at room temperature without any specifications.

Results and discussion

Single crystal structure of $Re(CO)_3$(PPOZ)Br

As mentioned in the Introduction part, a N–N ligand owing a typical electron-withdrawing group in its molecular structure was designed to improve the emissive performance of $Re(CO)_3$(PPOZ)Br. The successful synthesis of the Re(I) complex, as well as that of PPOZ ligand, can be proved by the single crystal structure shown in Fig. 1A. It can be seen that the pyridine group and the benzene group are connected to 1,3,4-oxadiazole group via two σ bonds. The free rotation of both σ bonds allows the three groups to form a large conjugation plane. The central Re(I) ion is surrounded by three CO groups, two N atoms from a PPOZ ligand and a Br atom, which means that it occupies the center of a distorted octahedral coordination environment. The selected structural parameters of this coordination sphere are summarized in Table 1, which confirms the distortion of the coordination environment around Re(I) center. The three bond length values shown in Table 1 are comparable with literature ones [17], however, they are slightly different from each other. It can be observed that Re–C(1) and Re–C(2) bond length values are similar to each other, while Re–C(2) bond is longer than both ones, which means that the Br atom localized at the opposite site of C(2) may slightly decrease the coordination ability of C(2). There is also a slight difference between the two Re–N bonds. Since Re–N(1) bond (2.165 Å) is shorter than Re–N(2) bond (2.228 Å), the coordination ability of N(1) atom from 1,3,4-oxadiazole group is then higher than that of N(2) atom from pyridine group. It is expected that the restricted conjugation chain and the electron-pushing O atom in 1,3,4-oxadiazole group are responsible for the increased coordination ability of N(1). In other words, the restricted conjugation chain limits the delocalization of N(1) lone pair, and its coordination ability is further enhanced by the neighboring electron-pushing O atom. In addition, the structural distortion may also be partially responsible for the bond length difference [17].

As for the bond angles listed in Table 1, their values also indicate the distortion of the coordination field. The bite angle of N–Re–N is only 73.25° which is quite smaller than literature values in tetrahedral fields (>80°) [14–17], indicating that the coordination environment in $Re(CO)_3$(PPOZ)Br is less congested than that in tetrahedral fields. We attribute the causation to the small steric hindrance of CO and Br ligands. Since the geometric relaxation of MLCT excited state is responsible for the major energy loss path, the less crowded coordination field may face more severe geometric relaxation [12–15]. On the positive side, the immobilization effect from polymer host can be confirmed with the elimination of ligand steric hindrance.

As above mentioned, PPOZ ligand takes a coplanar structure. The face-to-face π–π attraction between PPOZ ligands makes $Re(CO)_3$(PPOZ)Br molecules take a highly ordered array as shown in Fig. 1B, which is consistent with the literature report by Zhang and coworkers [12,15]. In this case, each PPOZ ligand aligns nearly parallel to each other, correspondingly, $Re(CO)_3$(PPOZ)Br molecules also adjust their orientation to meet the π–π attraction between PPOZ ligands. The intersection angle and the face-to-face

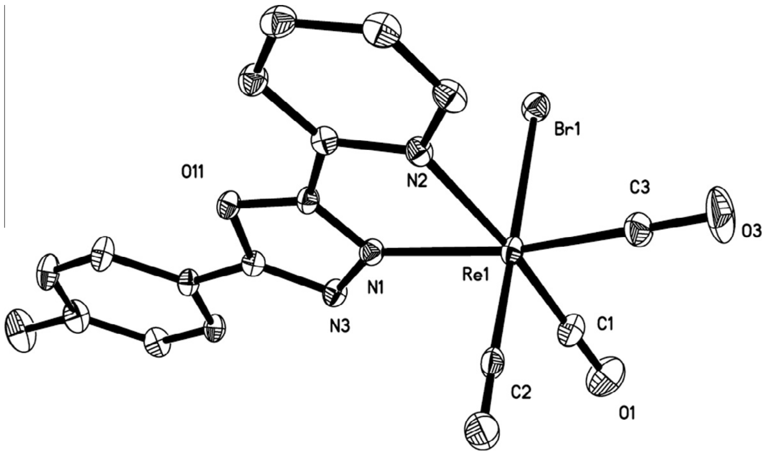

Fig. 1A. The single crystal structure of $Re(CO)_3$(PPOZ)Br. All hydrogen atoms are omitted for clarity.

Table 1
Selected structure parameters of $Re(CO)_3(PPOZ)Br$ obtained from single crystal.

Bond length	Å	Bond angle	°
Re–C(1)	1.886	N(1)–Re–N(2)	73.25
Re–C(2)	1.920	N(1)–Re–C(1)	99.41
Re–C(3)	1.890	N(2)–Re–C(3)	99.48
Re–Br(1)	2.615	N(1)–Re–Br(1)	84.80
Re–N(1)	2.165	N(2)–Re–Br(1)	86.37
Re–N(2)	2.228	N(1)–Re–C(2)	95.49
		N(2)–Re–C(2)	91.86

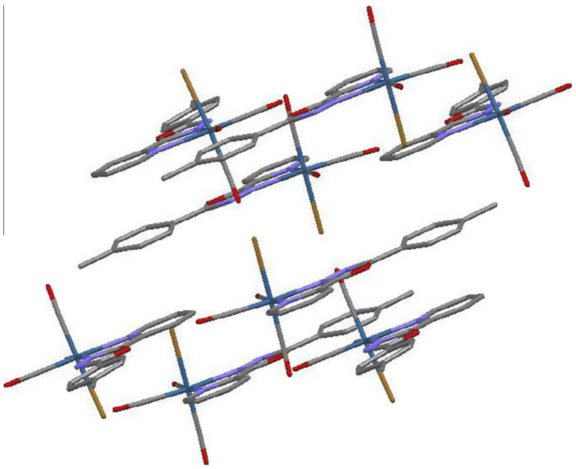

Fig. 1B. The face-to-face π–π attraction between PPOZ ligands in $Re(CO)_3(PPOZ)Br$ crystal.

distance between PPOZ ligands are only 1.72° and 3.257 Å, confirming the existence of face-to-face π–π attraction between PPOZ ligands. According to Zhang's statement [12,15], this highly ordered array can be considered as a rigid structure, where the MLCT excited state geometric relaxation can be effectively repressed, showing improved emissive performance such as increased emissive energy, longer excited state lifetime and higher emission yield. It is thus expected that $Re(CO)_3(PPOZ)Br$ crystal may also presents an improved emissive performance compared with that of diluted $Re(CO)_3(PPOZ)Br$ molecule.

Theoretical calculation and analysis on $Re(CO)_3(PPOZ)Br$

Since the photoinduced excitations and emissions involve electronic transitions between FMOs, it is thus necessary to get a clear understanding on the FMOs as well as the onset electronic transitions of $Re(CO)_3(PPOZ)Br$. TD-DFT calculation has been proved to be a powerful tool to reveal the electronic structure of transition metal complexes [12–15]. The percentage composition of the FMOs as well as that the first ten onset electronic transitions are summarized in Table 2. Similar to literature cases [12–15], the occupied FMOs of MOs 66–70 all own predominant metal character, admixed with some contributions from Br atom and CO groups. On the other hand, the unoccupied FMOs of MOs 71–73 are essentially π^* orbitals of PPOZ ligand. To get a visual understanding, two representative MOs of HOMO and LUMO are plotted as Fig. 2. Clearly, the electron cloud mainly distributes on Br atom and Re center on ground state. Upon excitation, the electron cloud localizes mainly on PPOZ ring, suggesting a charge transfer process. The first ten singlet excitations nearly all consist of electronic transitions from occupied FMOs to unoccupied ones, which means that they own a mixed character of metal-to-ligand-charge-transfer (MLCT $[d(Re) \rightarrow \pi^*(PPOZ)]$) and ligand-to-ligand-charge-transfer (LLCT). The excited state is usually derived from the onset electronic transition and thus should also be assigned as a mixed character of MLCT and LLCT. In addition, the electron-withdrawing group 1,3,4-oxadiazole is clearly involved in the photoinduced electronic transitions, and the emissive performance of $Re(CO)_3(PPOZ)Br$ is expected to be improved [15].

Table 2
Percentage composition of FMOs as well as the first ten onset electronic transitions.

MO/transition	Energy (eV)	Contribution (%)			
		Re	CO	PPOZ	Br
LUMO + 2(73)	−1.894	0.6	1.2	98.0	0.3
LUMO + 1(72)	−2.297	1.2	1.7	96.6	0.5
LUMO(71)	−3.157	4.2	4.1	89.6	2.0
HOMO(70)	−5.676	35.1	18.3	4.5	42.1
HOMO-1(69)	−5.796	27.7	14.1	9.9	48.2
HOMO-2(68)	−6.634	61.7	27.9	9.7	0.7
HOMO-3(67)	−6.947	33.5	14.5	20.2	31.7
HOMO-4(66)	−7.064	36.5	16.7	13.1	33.7
$S_0 \rightarrow S_1$	1.7671	70 → 71(98.6)			
$S_0 \rightarrow S_2$	1.9952	69 → 71(98.0)			
$S_0 \rightarrow S_3$	2.6692	68 → 71(98.5)			
$S_0 \rightarrow S_4$	2.7377	70 → 72(96.2)			
$S_0 \rightarrow S_5$	2.8585	69 → 72(97.6)			
$S_0 \rightarrow S_6$	3.0595	67 → 71(86.6)			
$S_0 \rightarrow S_7$	3.1813	70 → 73(94.5)			
$S_0 \rightarrow S_8$	3.2899	69 → 73(53.4)+66 → 71(37.1)			
$S_0 \rightarrow S_9$	3.3230	66 → 71(45.3)+ 69 → 73(44.6)			
$S_0 \rightarrow S_{10}$	3.6564	68 → 72(97.6)			

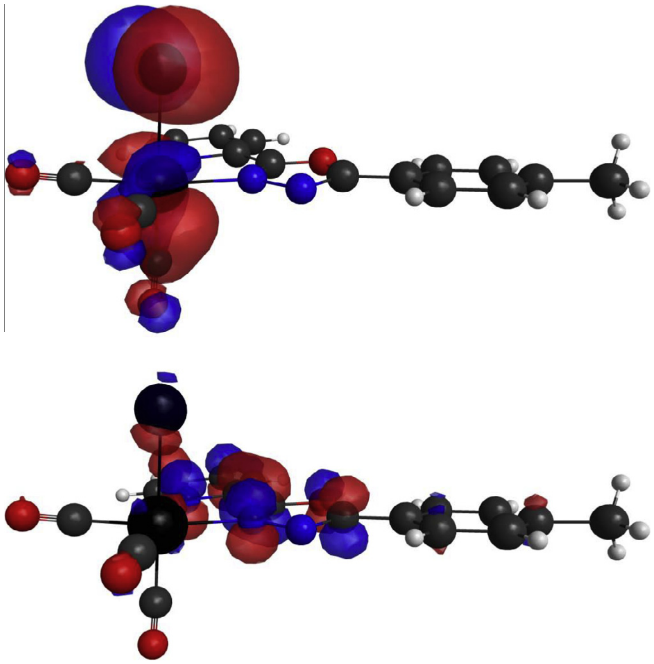

Fig. 2. The graphical presentations of two representative MOs of HOMO (up) and LUMO (down).

SEM and fluorescence microscopy images of PVP@$Re(CO)_3(PPOZ)Br$

As for the supporting host, it need to own enough mechanical strength, as well as good electrospinning property to meet the requirements for optoelectronic dopants such as porous structure and controllable morphology. Among the proposed candidates for electrospinning hosts, PVP has been widely used due to its advantages of uniform morphology, practicable mechanical strength and good compatibility with optoelectronic dopants [19]. In this paper, PVP is selected as the supporting host for Re(CO)$_3$(PPOZ)Br doped composite fibers. Four doping concentrations, 6 wt%, 10 wt%, 14 wt% and 16 wt%, are tried to systematically study the photophysical features of those composite fibers and correspondingly seek the optimal doping concentration. First, the morphology of those composite fibers can be directly seen from their SEM images. As shown in Fig. 3A, all electronspinning fibers are randomly distributed on the substrates, showing orderless arrangement. No branches have been observed for those composite fibers, showing smooth surface. The average diameter vales for those fibers are 90 nm for the 6 wt% sample, 100 nm for the 10 wt% sample, 110 nm for the 14 wt% sample and 100 nm for the 16 wt% sample, respectively. It is observed that the diameter is nearly independent of the doping concentration variation. No detectable phase separation can be observed, indicating PVP's good compatibility with Re(CO)$_3$(PPOZ)Br. Those fibers intercross with each other, resulting in a fibrous porous structure whose surface-to-volume ratio is two orders of magnitude higher than those of bulk materials, making them a shining host for optoelectronic dopants [19].

The successful doping and good compatibility with the dopant can also be confirmed by the representative fluorescence microscopy image of the 14 wt% sample shown in Fig. 3B. Clearly, there is yellow emission coming out from the composite fibers under Hg-lamp excitation, which means that the optoelectronic dopant Re(CO)$_3$(PPOZ)Br has been successfully doped into PVP host. We have above mentioned that there is face-to-face π–π stacking in Re(CO)$_3$(PPOZ)Br crystal. With the universal distribution in PVP host, the π–π stacking can be eliminated in those composite fibers, further confirming the immobilization effect from PVP host, which will be discussed in detail below.

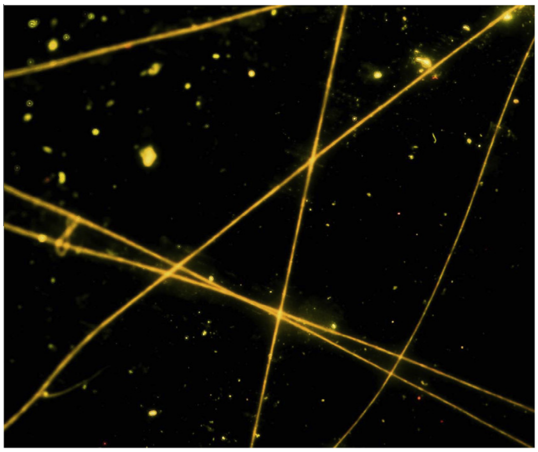

Fig. 3B. The representative fluorescence microscopy image of the 14 wt% sample.

Photophysical features of Re(CO)$_3$(PPOZ)Br and PVP@Re(CO)$_3$(PPOZ)Br

Absorption and diffuse reflection spectra

The electronic transition of Re(CO)$_3$(PPOZ)Br and the composite fibers can be presented by their absorption spectra. As a consequence, the absorption spectra (abs.) of Re(CO)$_3$(PPOZ)Br solution in CH_2Cl_2 with concentration of 1 μM, the four composite fibers and pure PVP are measured and shown in Fig. 4. Bulk Re(CO)$_3$(PPOZ)Br, however, is hard to take its absorption spectra since it is too thick for light to penetrate. Alternatively, its solid state diffuse reflection spectrum is then measured to evaluate its electronic transition. As shown in Fig. 4, the absorption spectrum for Re(CO)$_3$(PPOZ)Br dilute solution consists of two major regions, which are the high energy one ranging from 230 nm to 350 nm with triple peaks at 260 nm, 290 nm and 330 nm, and the low energy one ranging from 365 nm to 500 nm with broad peak around 395 nm, respectively. Considering their similar absorption energy and extinction coefficient with those of free ligands [16,17,19], the first one can be identified as the spin-allowed $\pi \rightarrow \pi^*$ transitions of PPOZ ligand. While the latter one can be tentatively attributed to absorption of MLCT and LLCT according to above theoretical calculation result. This assignment is consistent with MLCT and LLCT transitions' low extinction coefficients [13–16].

The four composite fibers present similar absorption spectra with that of Re(CO)$_3$(PPOZ)Br dilute solution, peaking at 240 nm, 290 nm and 337 nm, respectively, along with a broad band

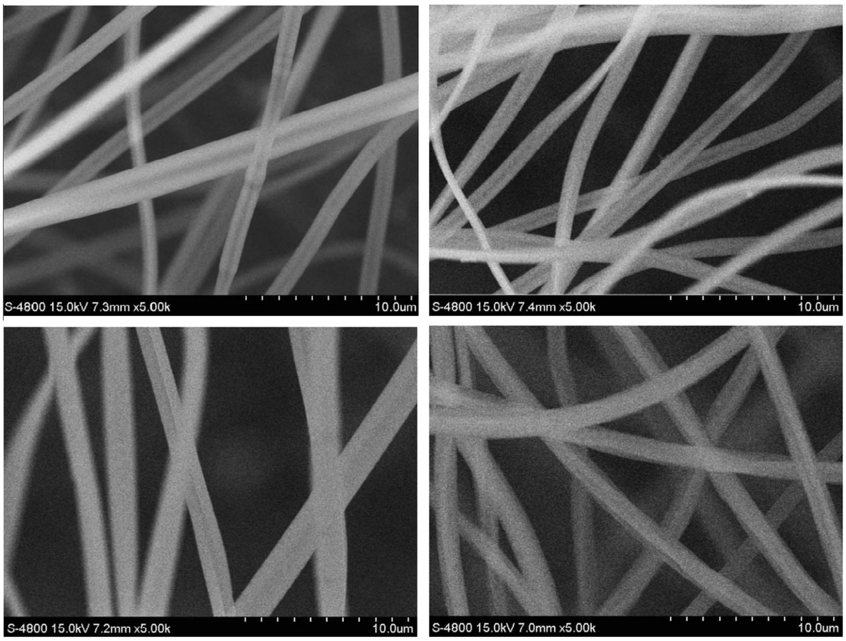

Fig. 3A. The SEM images of the 6 wt% sample (up left), the 10 wt% doped sample (up right), the 14 wt% doped sample (down left) and the 16 wt% doped sample (down right).

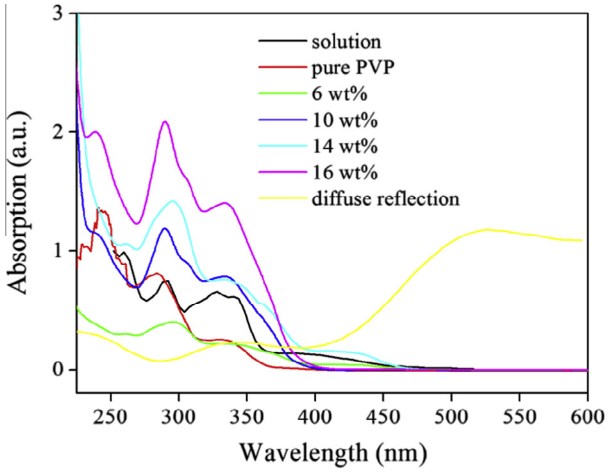

Fig. 4. The absorption spectra of $Re(CO)_3(PPOZ)Br$ solution in CH_2Cl_2 with concentration of 1 μM, the four composite fibers and pure PVP, along with the solid state diffuse reflection spectrum of bulk $Re(CO)_3(PPOZ)Br$.

extending to ∼450 nm. The first band at 240 nm is quite similar to the absorption peak of pure PVP, while the latter two ones can be recognized as the absorption peaks of $Re(CO)_3(PPOZ)Br$. After being doped into PVP host, $Re(CO)_3(PPOZ)Br$ shows nearly identical absorption feature with that of dilute solution without any newly-generated peaks or shoulder bands. It is thus concluded that there is no strong interaction between dopant molecules and PVP host. $Re(CO)_3(PPOZ)Br$ molecules are merely trapped and immobilized in PVP matrix.

As for bulk $Re(CO)_3(PPOZ)Br$, its solid state diffuse reflection spectrum owns low reflection over a wide region ranging from 230 nm to 400 nm, with a typical valley at 290 nm, which is in consistent with the strongest absorption of $Re(CO)_3(PPOZ)Br$ dilute solution. Similarly, no newly-generated bands are observed. It is thus concluded that the electronic transitions of $Re(CO)_3(PPOZ)Br$ are independent of its existing status: diluted in solution, condensed in solid state or immobilized in PVP host.

Emissive spectra

The emissive spectra for the four composite samples, $Re(CO)_3(PPOZ)Br$ solution in CH_2Cl_2 with concentration of 1 μM and bulk $Re(CO)_3(PPOZ)Br$ are shown in Fig. 5. In solution, $Re(CO)_3(PPOZ)Br$ exhibits yellow emission centering at 563 nm with FWHM value as large as 87 nm. Here, FWHM means full-width-at-half-maximum. The emission spectrum is broad, showing no vibronic progression, suggesting the charge transfer nature of the emissive state. This observation is in consistent with above theoretical calculation result and literature reports [12,14,15,17]. In solid state, $Re(CO)_3(PPOZ)Br$ emission moves to 572 nm with FWHM value of 93 nm The red shift can be attributed to the aggregation of the excited states [15]. It has been above pointed out that there is π–π stacking within solid $Re(CO)_3(PPOZ)Br$ crystal, which is believed to be effective on repressing MLCT excited state relaxation and thus improving emissive performance [15]. Compared with the emission spectrum in solution, it can be observed, however, that such π-π stacking may be plain in repressing the excited state relaxation since the crystal emissive state shows a decreased energy and widened spectrum.

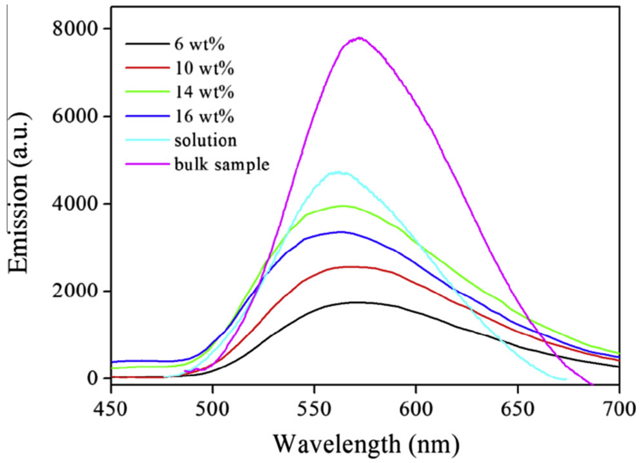

Fig. 5. The emissive spectra for the four composite samples, $Re(CO)_3(PPOZ)Br$ solution in CH_2Cl_2 with concentration of 1 μM and bulk $Re(CO)_3(PPOZ)Br$.

After being doped into PVP host, $Re(CO)_3(PPOZ)Br$ emission shifts to 573 nm for the 6 wt% sample, 568 nm for the 10 wt% sample, 562 nm for the 14 wt% sample and 563 nm for the 16 wt% sample, respectively. Their FWHM values are 115 nm, 114 nm, 116 nm and 118 nm, respectively. The emission blue shift and the widened spectra indicate that the immobilization in PVP matrix can repress the MLCT geometric relaxation and stabilize the emissive state. As suggested by literature reports, the geometric relaxation is the main causation for energy loss and inradiative decay path of MLCT excited states [12,15]. When $Re(CO)_3(PPOZ)Br$ molecules are doped into PVP host, they are also immobilized in the polymer matrix and not free to distort their structures. With the excited state geometric relaxation effectively repressed, it is not surprised to see the emission blue shift from PVP doped fibers. Since the excited state can be stabilized by PVP host, the emission spectra are consequently widened. It seems that the immobilization in polymer matrix is even more effective on repressing the geometric relaxation than π–π stacking does, where the small steric hindrance of CO group and Br atom should be blamed to be responsible.

Excited state decay dynamics

Aiming at a deeper understanding on the immobilization influence on the excited state, its lifetimes upon various existing statuses are measured and discussed as follows. The excitation spectrum of $Re(CO)_3(PPOZ)Br$ is firstly recorded to ensure effective excitation. As shown in Fig. 6, the excited state of $Re(CO)_3(PPOZ)Br$ follows single exponential decay mode regardless of its existing status, with decay times of 1.80 μs for $Re(CO)_3(PPOZ)Br$ solution, 3.13 μs for bulk $Re(CO)_3(PPOZ)Br$, 4.47 μs for the 6 wt% sample,

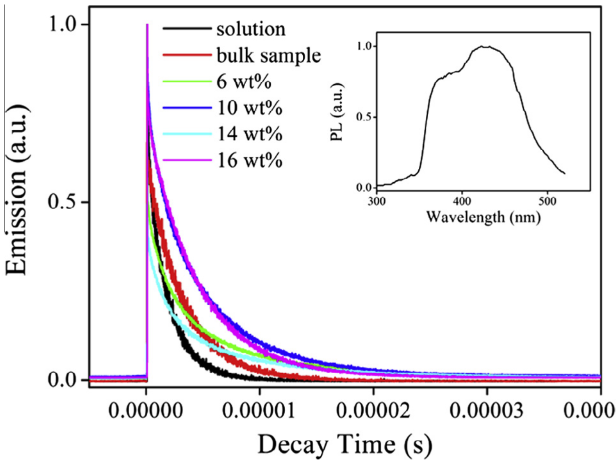

Fig. 6. The emission decay characters of the four composite fibers, $Re(CO)_3(PPOZ)Br$ solution in CH_2Cl_2 with concentration of 1 μM and bulk $Re(CO)_3(PPOZ)Br$. Inset: the excitation spectrum of $Re(CO)_3(PPOZ)Br$ solution.

4.79 μs for the 10 wt% sample, 4.88 μs for the 14 wt% sample and 4.42 μs for the 16 wt% sample, respectively. The single exponential decay mode suggests that all excited states localize in homogenous environment. As for $Re(CO)_3(PPOZ)Br$ solution, the molecules in dilute solution are surrounded by solvent molecules. They are thus free to distort their structure and to lose excited state energy, resulting in the shortest excited state lifetime of 1.80 μs. In condensed state, the excited state geometric relaxation of $Re(CO)_3$ (PPOZ)Br may be partially repressed by the π–π stacking above mentioned, leading to a longer excited state lifetime of 3.13 μs. When $Re(CO)_3(PPOZ)Br$ is doped into polymer host, the immobilization in PVP matrix effectively represses the excited state geometric relaxation, causing the even longer excited state lifetimes of the four composite fibers. Above comparison provides an evidence for the fact that the excited state geometric relaxation can be effectively repressed by doping $Re(CO)_3(PPOZ)Br$ into PVP matrix.

Although the excited state lifetimes of the four composite fibers are similar to each other, it seems that the excited state lifetime firstly increases with the increasing doping concentration, showing a maximum value when the doping concentration is as high as 14 wt%. Upon an even higher doping concentration of 16 wt%, the excited state lifetime tends to decrease. Apparently, 14 wt% is the optimal doping concentration. Bothe higher or lower doping concentrations can decrease the excited state lifetime, which may be explained as follows. The emissive intensity of the composite fibers clearly depends on the doping amount of $Re(CO)_3(PPOZ)Br$ molecules, which means that the higher the doping concentration is, the stronger the emissive intensity becomes. However, when the doping concentration is more than enough, the aggregation also becomes serious, correspondingly, the strong self-quenching and self-absorption may quench the excited state, leading to the decreased excited state lifetime.

Photostability

To get a further understanding on the photostability difference between bulk sample and composite fibers, the emission intensity variations of the four composite fibers and the bulk sample upon continuous radiation are given in Fig. 7. The emission of bulk $Re(CO)_3(PPOZ)Br$ decreases greatly with increasing radiation time, suggesting that the photostability of bulk $Re(CO)_3(PPOZ)Br$ is poor since bulk material directly accept the excitation energy. We attribute the emission intensity decrease to the photo-oxidization and photochemical breakdown of $Re(CO)_3(PPOZ)Br$ molecular structure. As for the four composite fibers, their emission intensity remains well with increasing radiation time, suggesting that the photostability of the composite fibers is improved compared with that of bulk $Re(CO)_3(PPOZ)Br$, which can be explained as follows. When being doped into polymer host, $Re(CO)_3(PPOZ)Br$ molecules are protected by the surrounding PVP framework which may act as an energy-absorbing antenna. The excitation energy can be firstly absorbed by the energy-absorbing antenna without directly exciting $Re(CO)_3(PPOZ)Br$ molecules. Thus, the photo-oxidization and photochemical breakdown can be avoided, leading to the improved photostability. In addition, it can be seen that the photostability of the composite fibers decreases with the increasing doping concentration. It is expected that the increasing aggregation between $Re(CO)_3(PPOZ)Br$ molecules may compromise the photostability of the composite fibers. On the positive side, the photostability of the composite fibers is found to be largely improved compared with that of bulk sample, suggesting that PVP can be developed as a promising host for composite fibers by repressing the MLCT excited state geometric relaxation and improving the photostability.

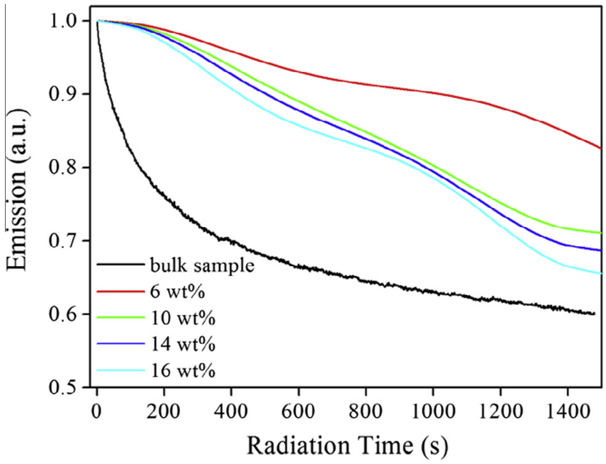

Fig. 7. The emission intensity variations of the four composite fibers and the bulk $Re(CO)_3(PPOZ)Br$ upon continuous radiation.

Conclusion

To sum up, we synthesized and characterized a Re(I) complex $Re(CO)_3(PPOZ)Br$ whose diamine ligand was composed of an electron-withdrawing oxadiazole group. Its geometric and electronic structures were confirmed and revealed by single crystal structure analysis and DFT calculation. $Re(CO)_3(PPOZ)Br$ took a traditional coordination pattern similar to literature cases. The excited state owned a mixed character of MLCT and LLCT which suffered from geometric relaxation. In order to repress the geometric relaxation and thus improve the emissive performance, $Re(CO)_3(PPOZ)Br$ was doped into PVP host via electrospinning to construct composite fibers. The photophysical features of the final composite fibers were compared with those of bulk sample. Data suggested that the composite fibers owned blue-shifted emission, longer excited state lifetime and better photostability, owing to the effective repression of the geometric relaxation. In other words, the immobilization in PVP matrix was effective on repressing the MLCT excited state geometric relaxation, showing improved emissive performance. Considering that MLCT geometric relaxation is the major energy loss of excited state, it is expected that the polymer immobilization effect might be an universal phenomenon. This conclusion may be used for future design of one dimensional nanostructures for optoelectronic applications. For further efforts, the combination of other transition metal complexes and polymer host should be carried out to testify the universality of this effect.

Acknowledgments

The author gratefully thank the financial support from the University Provincial Natural Science Research Key Project of Anhui Province, China (Grant No. KJ2011Z231).

References

[1] G.M. Kim, A. Wutzler, H.J. Radusch, G.H. Michler, P. Simon, R.A. Sperling, W.J. Parak, Chem. Mater. 17 (2005) 4949–4957.
[2] L. Feng, S. Li, H. Li, J. Zhai, Y. Song, L. Jiang, D. Zhu, Angew. Chem. Int. Ed. 41 (2002) 1221–1223.
[3] J. Hartgerink, E. Beniash, S. Stupp, Science 294 (2001) 1684–1688.
[4] D. Reneker, I. Chun, Nanotechnology 7 (1996) 216–223.
[5] J.A. Matthews, G.E. Wnek, D.G. Simpson, G.L. Bowlin, Biomacromolecules 3 (2002) 232–238.
[6] A.C. Patel, S.X. Li, C. Wang, W.J. Zhang, Y. Wei, Chem. Mater. 19 (2007) 1231–1238.
[7] K.E. Erkkila, D.T. Odom, J.K. Barton, Chem. Rev. 99 (1999) 2777–2796.
[8] C.A. Bignozzi, R. Argazzi, C.J. Kleverlaan, Chem. Soc. Rev. 29 (2000) 87–96.
[9] V.W.W. Yam, B. Li, Y. Yang, B.W.K. Chu, K.M.-C. Wong, K.K. Cheung, Eur. J. Inorg. Chem. 22 (2003) 4035–4042.

[10] S. Ranjan, S.Y. Lin, K.C. Hwang, Y. Chi, W.L. Ching, C.S. Liu, Y.T. Tao, C.H. Chien, S.M. Peng, G.H. Lee, Inorg. Chem. 42 (2003) 1248–1255.

[11] F. Li, M. Zhang, J. Feng, G. Cheng, Z.J. Wu, Y.G. Ma, S.Y. Liu, Appl. Phys. Lett. 83 (2003) 365–367.

[12] L. Zhang, B. Li, Z. Su, Langmuir 25 (2009) 2068–2074.

[13] L. Zhang, B. Li, J. Lumin. 129 (2009) 1304–1308.

[14] L. Yang, J.K. Feng, A.M. Ren, M. Zhang, Y.G. Ma, X.D. Liu, Eur. J. Inorg. Chem. 10 (2005) 1867–1879.

[15] L. Zhang, S. Yue, B. Li, D. Fan, Inorg. Chim. Acta 384 (2012) 225–232.

[16] L. Shi, B. Li, S. Yue, D. Fan, Sensor Actuat. B Chem. 137 (2009) 386–392.

[17] Z. Si, X. Li, X. Li, H. Zhang, J. Organomet. Chem. 694 (2009) 3742–3748.

[18] H.Q. Yu, H.W. Song, G.H. Pan, S.W. Li, Z.X. Liu, X. Bai, T. Wang, S.Z. Lu, H.F. Zhao, J. Lumin. 124 (2007) 39–44.

[19] Y. Wang, B. Li, Y. Liu, L. Zhang, Q. Zuo, L. Shi, Z. Su, Chem. Commun. 39 (2009) 5868–5870.